One and two charge stripping reactions in the $^{12}C+^{197}Au$ and $^{16}O+^{197}Au$ systems at large distances

D. Tomasi, J. O. Fernández Niello, A. J. Pacheco, D. Abriola, J. E. Testoni, A. O. Macchiavelli, O. A. Capurro, D. E. DiGregorio, M. di Tada, G. V. Martí, and I. Urteaga

Laboratorio TANDAR, Departamento de Física, Comisión Nacional de Energía Atómica, Avenida del Libertador 8250, 1429 Buenos Aires, Argentina

(Received 11 January 1996)

One- and two-charge-transfer reactions were studied in the $^{12}C+^{197}Au$ and $^{16}O+^{197}Au$ systems at bombarding energies around the Coulomb barrier. Transfer probabilities for the same Coulomb reduced radius, extracted from angular distribution measurements, show a strong dependence on the bombarding energy and are interpreted within a semiclassical model. Quasielastic scattering data are analyzed in terms of an energy-dependent optical model. [S0556-2813(96)01608-1]

PACS number(s): 25.70.Hi, 24.10.Ht, 25.70.Bc

I. INTRODUCTION

Heavy-ion-induced transfer reactions at bombarding energies close to the Coulomb barrier are a subject of current interest in the field of nuclear reactions in the last years. Particular attention has been concentrated in connection with the behavior of the transfer probability as a function of the distance of closest approach when one or two neutrons are involved in the reaction [1–3].

A deviation of the behavior of the transfer probabilities from the predictions of a simple semiclassical description (a barrier penetration model) when two neutrons are transferred has been reported previously [4–6]. Several recent experiments have pointed out possible deviations from the tunneling picture. In some cases, the observed anomalies were linked to interference effects between transfer to the ground-state band and transfer to bands of other intrinsic states [6,7].

In order to investigate to what extent these effects are also present in charge-transfer reactions we have examined the $^{12}C+^{197}Au$ and $^{16}O+^{197}Au$ systems at energies close to the Coulomb barrier where semiclassical approaches are expected to be valid. Transfer reactions in these systems have already been studied by Yokoyama *et al.* [8] and Eyal *et al.* [9] at energies well above the barrier.

Detailed measurements of angular distributions of the ejectiles at different bombarding energies have been performed as well as particle-gamma coincidence in order to achieve mass discrimination. In Sec. II the experimental setup and data analysis are described. Section III addresses the semiclassical calculations of transfer probabilities. An energy-dependent optical model analysis of the quasielastic scattering data obtained in this study is also presented in this section. Section IV summarizes the main results of this investigation.

II. EXPERIMENTAL METHOD

A. Experimental setup

Measurements were carried out at the 20 UD tandem accelerator of the TANDAR Laboratory in Buenos Aires. Targets of ^{197}Au (90 $\mu g/cm^2$ thick) were bombarded with ^{12}C and ^{16}O projectiles at energies ranging from 56 to 82 MeV and from 74 to 110 MeV, respectively. The calculated Coulomb barriers in the laboratory frame are 57 MeV for $^{12}C+^{197}Au$ and 77 MeV for $^{16}O+^{197}Au$ [10].

Two different experimental arrangements were used in this work. In the first experiment, angular distributions of transferred particles for both systems have been measured using a telescope detector consisting of a gas ionization chamber followed by a solid-state position-sensitive detector. Two-dimensional ΔE-E_{res} spectra for charge identification, as well as energy spectra for fragments with different atomic numbers, were obtained in the laboratory angular range $\theta=35°-165°$. Absolute cross sections were obtained by normalizing the transfer yields to the elastic scattering yield measured in two monitor detectors placed at $\theta=\pm 30°$ relative to the beam direction.

In a second complementary experiment, the reaction channels were identified by characteristic gamma-ray transitions measured in coincidence with the scattered projectile-like particles. For this purpose two telescopes, each consisting of two surface barrier detectors, were placed at different angular positions and a HP-Ge counter was placed at 90° with respect to the beam direction. The absence of strongly converted low-lying transitions in nuclei around the ^{197}Au isotope makes this technique adequate. A thick ^{197}Au target of about 1 mg/cm^2 was used in order to obtain a satisfactory rate of coincident events.

B. Analysis

Figure 1 shows a ΔE-E_{res} scatter plot corresponding to the reaction $^{12}C+^{197}Au$ at a bombarding energy $E_{lab}=65$ MeV. The predominant reaction channels were associated with charge stripping reactions ($Z=4, 5$). No evidence of charge pickup ($Z=7, 8$) was found, in agreement with optimum Q-value considerations. From these plots and gating on each Z, Q-value spectra were produced assuming binary kinematics. In order to test the sensitivity of these Q-value spectra with respect to the mass of the detected particle, several calculations were performed assuming different values of mass number A for each atomic number Z. Typically, variations of ± 1 amu result in a variation of ± 0.4 MeV. The

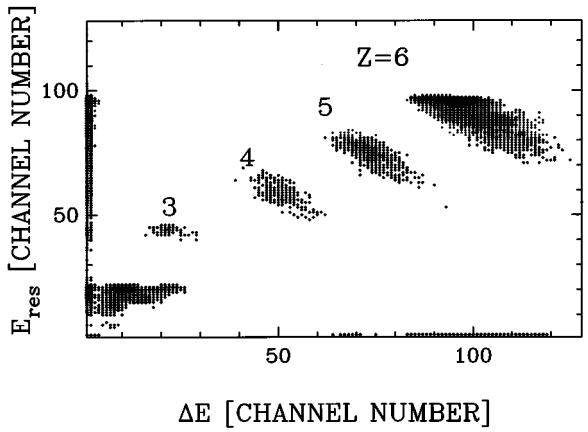

FIG. 1. Scatter plot ΔE-$E_{\rm res}$ obtained for the reaction ^{12}C+^{197}Au at $E_{\rm lab}$=65 MeV and Θ=112.1°.

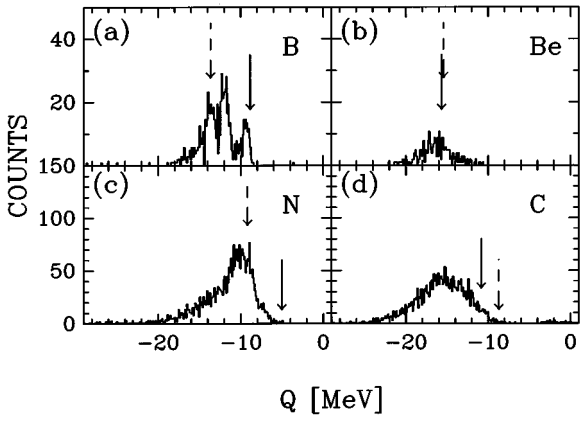

FIG. 3. Q-value spectra of the projectilelike fragments. (a) and (b) correspond to ^{12}C projectiles at Θ=112.1° and $E_{\rm lab}$=65 MeV, while (c) and (d) correspond to ^{16}O projectiles at Θ=109.1° and $E_{\rm lab}$=85 MeV. The labels indicate the detected ejectiles. In the cases of one-charge-transfer reactions [(a) and (c)], the solid and dashed arrows indicate the value of Q_{gg} for one-proton and one-deuteron stripping, respectively. For two-charge-transfer reactions [(b) and (d)] the solid and dashed arrows indicate the value of Q_{gg} for two-proton and α stripping, respectively.

procedure to obtain Q-value spectra was evaluated by checking that the elastic peaks are centered at $Q\sim 0$ MeV.

By setting appropriate gates on the ΔE-$E_{\rm res}$ plots, Q-value spectra and gamma ray energy spectra in coincidence with different atomic numbers Z were obtained. The simultaneous analysis of Q-value and gamma-ray energy spectra was used for a tentative identification of the various reaction channels, as is discussed in what follows.

1. Gamma-ray energy spectra

Figure 2 shows gamma-ray spectra gated on projectilelike fragments with Z=5 and Z=4 for the ^{12}C+^{197}Au system at $E_{\rm lab}$=65 MeV. The spectrum for the transfer of one charge [Fig. 2(a)] shows peaks at E_γ=411.8, 587.2, and 636.7 keV, corresponding to the $2^+\rightarrow 0^+$, $5^-\rightarrow 4^+$, and the $4^+\rightarrow 2^+$ transitions, respectively, in the ^{198}Hg nucleus [11], which indicates the occurrence of one-proton transfer. No evidence was found of the 158.4 keV gamma ray corresponding to an $E2$ transition from the first excited state to the ground state of ^{199}Hg, which would correspond to the one-deuteron stripping reaction. Similar conclusions can be drawn from the analysis of the gamma-ray spectra obtained at other energies, as well as from spectra measured for the ^{16}O+^{197}Au system.

For the ^{12}C+^{197}Au reaction, the gamma-ray spectrum corresponding to Z=4 [Fig. 2(b)] shows only one relatively strong peak at E_γ=366.7 keV produced by the $3/2^+\rightarrow 1/2^+$ transition in ^{199}Tl [11], the heaviest reaction product of the two-proton stripping channel. Although the transfer of α particles cannot be ruled out, this channel is not present in these data because the corresponding projectilelike fragment ^{8}Be decays promptly and, therefore, it does not trigger the acquisition. The same remark is valid for the two-proton–one-neutron reaction channel because the excited states of ^{9}Be decay by particle emission. The transfer to the ground state

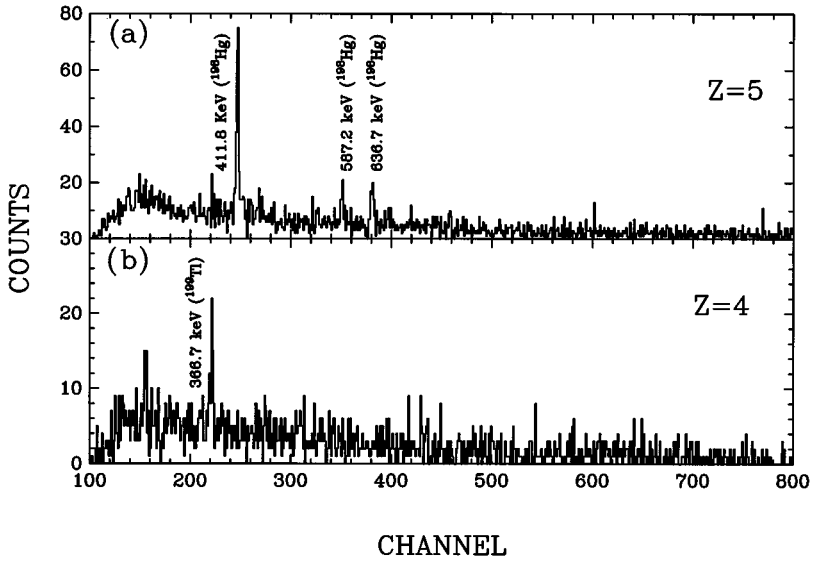

FIG. 2. Gamma-ray spectra in coincidence with Z=4 and Z=5 fragments for the ^{12}C+^{197}Au system at $E_{\rm lab}$=65 MeV and Θ=112.1°.

TABLE I. Differential transfer cross sections for one- and two-charge transfer in the $^{16}O+^{197}Au$ system.

Θ [deg]	$d\sigma/d\Omega^{\Delta Z=1}$ [mb/sr]	$d\sigma/d\Omega^{\Delta Z=2}$ [mb/sr]
$E_{lab}=110$ MeV		
39.3	6.3 ± 0.3	20 ± 1
43.5	7.5 ± 0.4	27 ± 1
47.8	11.3 ± 0 .5	34 ± 2
49.8	23 ± 1	33 ± 2
54.0	25 ± 1	36 ± 2
55.0	29 ± 2	29 ± 1
58.2	28 ± 2	29 ± 1
59.2	26 ± 1	26 ± 1
63.4	21 ± 1	19 ± 1
70.7	9.8 ± 0.5	10.4 ± 0.5
74.8	5.2 ± 0.3	7.1 ± 0.4
78.9	3.0 ± 0.2	4.4 ± 0.2
81.0	2.3 ± 0.1	3.2 ± 0.2
85.1	1.58 ± 0.08	2.3 ± 0.1
89.1	0.73 ± 0.04	1.48 ± 0.07
$E_{lab}=90$ MeV		
65.6	1.24 ± 0.06	5.0 ± 0.2
69.8	1.81 ± 0.09	7.0 ± 0.3
73.9	3.2 ± 0.2	9.8 ± 0.5
81.1	8.2 ± 0.4	12.0 ± 0.6
85.2	9.6 ± 0.5	12.8 ± 0.6
89.2	9.6 ± 0.5	10.8 ± 0.5
91.8	13.5 ± 0.7	12.7 ± 0.6
95.5	11.7 ± 0.6	10.7 ± 0.5
99.8	9.6 ± 0.5	10.3 ± 0.5
103.7	7.9 ± 0.4	8.4 ± 0.4
107.5	5.9 ± 0.3	6.5 ± 0.3
111.3	3.4 ± 0.2	4.4 ± 0.2
114.9	2.6 ± 0.1	3.2 ± 0.2
117.9	2.2 ± 0.1	2.8 ± 0.1
$E_{lab}=85$ MeV		
81.1	0.65 ± 0.03	3.1 ± 0.1
85.2	1.22 ± 0.06	4.2 ± 0.2
89.2	2.1 ± 0.1	5.0 ± 0.2
97.4	7.1 ± 0.4	6.6 ± 0.3
101.1	7.7 ± 0.4	7.4 ± 0.4
105.3	7.9 ± 0.4	7.7 ± 0.4
109.1	7.6 ± 0.4	7.2 ± 0.4
112.9	6.8 ± 0.3	6.3 ± 0.3
117.0	5.8 ± 0.3	6.2 ± 0.3
120.7	5.3 ± 0.3	5.6 ± 0.3
124.9	4.4 ± 0.2	5.2 ± 0.3
128.7	3.4 ± 0.2	4.1 ± 0.2
132.4	2.9 ± 0.2	3.6 ± 0.2
136.1	2.9 ± 0.2	3.8 ± 0.2
139.5	2.6 ± 0.1	3.7 ± 0.2
141.1	2.0 ± 0.1	2.8 ± 0.1
143.1	2.1 ± 0.1	3.2 ± 0.2
146.3	1.71 ± 0.09	2.5 ± 0.1

TABLE I. (*Continued*.)

Θ [deg]	$d\sigma/d\Omega^{\Delta Z=1}$ [mb/sr]	$d\sigma/d\Omega^{\Delta Z=2}$ [mb/sr]
$E_{lab}=80$ MeV		
110.1	3.1 ± 0.1	2.9 ± 0.2
113.8	3.5 ± 0.2	3.2 ± 0.2
117.9	4.7 ± 0.2	3.8 ± 0.2
121.6	4.9 ± 0.2	4.1 ± 0.2
125.4	5.0 ± 0.2	4.1 ± 0.2
129.4	5.4 ± 0.3	4.8 ± 0.2
133.0	5.2 ± 0.3	4.3 ± 0.2
137.0	5.4 ± 0.3	4.9 ± 0.2
140.6	4.9 ± 0.2	4.4 ± 0.2
144.3	4.6 ± 0.2	4.2 ± 0.2
148.3	4.9 ± 0.2	4.5 ± 0.2
151.8	4.1 ± 0.2	3.8 ± 0.2
154.6	4.1 ± 0.2	4.1 ± 0.2
$E_{lab}=77$ MeV		
105.9	1.39 ± 0.07	
109.8	1.56 ± 0.08	0.10 ± 0.01
113.7	1.86 ± 0.09	0.37 ± 0.02
120.2	2.9 ± 0.1	0.89 ± 0.04
124.0	3.4 ± 0.2	1.37 ± 0.07
127.9	3.3 ± 0.2	1.53 ± 0.08
134.8	3.9 ± 0.2	2.3 ± 0.1
138.6	4.7 ± 0.2	2.9 ± 0.1
142.3	4.7 ± 0.2	3.1 ± 0.2
146.2	3.8 ± 0.2	3.2 ± 0.2
149.9	4.6 ± 0.2	3.4 ± 0.2
153.6	4.5 ± 0.2	3.4 ± 0.2
$E_{lab}=76$ MeV		
122.7	0.96 ± 0.05	0.25 ± 0.01
126.3	1.03 ± 0.05	0.32 ± 0.02
130.4	1.39 ± 0.07	0.59 ± 0.03
134.0	1.62 ± 0.08	0.79 ± 0.04
137.7	1.78 ± 0.09	0.89 ± 0.04
141.7	2.3 ± 0.1	1.27 ± 0.06
145.2	2.4 ± 0.1	1.22 ± 0.06
149.2	2.9 ± 0.2	1.77 ± 0.09
152.8	3.1 ± 0.2	1.87 ± 0.09
156.4	2.9 ± 0.1	1.85 ± 0.09
$E_{lab}=75$ MeV		
120.8	0.09 ± 0.01	
124.6	0.19 ± 0.01	
128.4	0.22 ± 0.01	
135.1	0.30 ± 0.02	0.24 ± 0.01
138.9	0.53 ± 0.03	0.36 ± 0.02
142.6	0.62 ± 0.03	0.48 ± 0.02
145.8	1.02 ± 0.05	0.48 ± 0.02
149.5	1.27 ± 0.06	0.72 ± 0.04
153.3	1.27 ± 0.06	0.90 ± 0.04

TABLE I. (*Continued*.)

Θ [deg]	$d\sigma/d\Omega^{\Delta Z=1}$ [mb/sr]	$d\sigma/d\Omega^{\Delta Z=2}$ [mb/sr]
$E_{lab}=74$ MeV		
134.8	0.18 ± 0.01	0.04 ± 0.01
138.6	0.24 ± 0.01	0.09 ± 0.01
142.3	0.31 ± 0.02	0.14 ± 0.01
146.3	0.49 ± 0.02	0.21 ± 0.01
150.1	0.71 ± 0.04	0.31 ± 0.02
153.8	0.93 ± 0.05	0.39 ± 0.02

of ^{9}Be appears to be very unlikely since the 147.6-keV gamma ray in ^{200}Tl is not observed. Again, similar spectra were obtained for all the studied energies for both systems.

2. Q-value spectra

The information furnished by the gamma-ray spectra regarding mass identification is complemented by the Q-value spectra. As an example, Fig. 3 shows Q-value spectra gated on $Z=4$ and 5 (6 and 7) for ^{12}C (^{16}O) projectiles.

The Q values for the transitions to the ground state of various exit channels, Q_{gg}, are shown by arrows. The energy resolution of the spectra was about 1 MeV. In the case of $\Delta Z=1$, Figs. 3(a) and 3(c), the energy spectra are in reasonable agreement with those corresponding to the one-proton stripping for both projectiles. Transfer of one deuteron is negligible for ^{12}C projectiles at the lowest bombarding energy (56 MeV) but this channel cannot be in general ruled out, particularly at the highest bombarding energies for ^{16}O projectiles. However, as was previously discussed, the absence of low-lying ^{199}Hg transitions in the gamma-ray spectra does not support the presence of this channel. In the case of $\Delta Z=2$, Fig. 3(b) corresponding to the ^{12}C projectile shows only two-proton-transfer events taking into account the arguments mentioned above. On the other hand, the events shown in Fig. 3(d) (^{16}O projectile) are compatible with two-proton as well as with alpha pickup Q values.

III. RESULTS

Differential cross sections for charge-transfer reactions were obtained (see Tables I and II) by grouping events in angular bins of $\Delta\theta=4°$. These angular distributions are bell shaped (see Fig. 4) and they peak slightly above the grazing angle. Total cross sections for one- and two-charge transfer in ^{12}C+^{197}Au and ^{16}O+^{197}Au systems (see Fig. 5 and Table III) were obtained by integration of a smooth curve interpolating the experimental points for each angular distribution. The quoted error bars include the statistical uncertainties and an estimate of the systematic errors. Systematic errors arise from the absolute normalization based on Rutherford scattering (<2%) and the statistical errors come from the determination of the peak areas (<3%). The bombarding energy was determined with an accuracy of 1%.

Figure 5 shows that the transfer cross sections are quite constant at energies above the Coulomb barrier and they exhibit a sharp falloff as the energy decreases below the bar-

TABLE II. Differential transfer cross sections for one- and two-charge transfer in the ^{12}C+^{197}Au system.

Θ [deg]	$d\sigma/d\Omega^{\Delta Z=1}$ [mb/sr]	$d\sigma/d\Omega^{\Delta Z=2}$ [mb/sr]
$E_{lab}=82$ MeV		
49.0	9.3 ± 0.5	8.4 ± 0.4
53.1	12.3 ± 0.6	7.9 ± 0.4
57.3	14.4 ± 0.7	7.5 ± 0.4
69.8	7.4 ± 0.4	3.5 ± 0.2
73.9	4.2 ± 0.2	2.0 ± 0.1
78.0	3.1 ± 0.1	1.48 ± 0.07
85.0	1.6 ± 0.1	0.81 ± 0.04
89.1	0.89 ± 0.04	0.44 ± 0.02
93.1	0.61 ± 0.03	0.36 ± 0.02
99.9	0.31 ± 0.02	0.15 ± 0.01
103.9	0.19 ± 0.01	0.09 ± 0.01
107.8	0.14 ± 0.01	0.07 ± 0.01
$E_{lab}=70$ MeV		
71.9	3.1 ± 0.2	2.5 ± 0.1
75.7	4.6 ± 0.2	2.5 ± 0.1
80.1	6.4 ± 0.3	3.3 ± 0.2
83.9	7.0 ± 0.3	2.7 ± 0.1
87.9	6.5 ± 0.3	2.5 ± 0.1
92.1	6.5 ± 0.3	2.8 ± 0.1
95.9	5.2 ± 0.3	2.0 ± 0.1
100.1	4.0 ± 0.2	1.9 ± 0.1
103.9	3.1 ± 0.2	1.33 ± 0.07
107.8	2.5 ± 0.1	1.07 ± 0.05
112.0	1.80 ± 0.09	0.91 ± 0.05
115.6	1.58 ± 0.08	0.75 ± 0.04
118.7	1.11 ± 0.06	0.60 ± 0.03
$E_{lab}=65$ MeV		
92.3	2.6 ± 0.1	1.19 ± 0.06
96.1	3.1 ± 0.2	1.35 ± 0.07
100.3	3.7 ± 0.2	1.49 ± 0.07
104.1	3.7 ± 0.2	1.43 ± 0.07
108.0	3.8 ± 0.2	1.67 ± 0.08
112.1	3.8 ± 0.2	1.60 ± 0.08
115.8	3.3 ± 0.2	1.41 ± 0.07
119.9	3.0 ± 0.2	1.44 ± 0.07
123.7	2.4 ± 0.1	1.03 ± 0.05
127.4	2.3 ± 0.1	0.97 ± 0.05
131.5	1.87 ± 0.09	0.94 ± 0.05
135.1	1.73 ± 0.09	0.82 ± 0.04
138.1	1.55 ± 0.08	0.82 ± 0.04
$E_{lab}=60$ MeV		
112.2	0.69 ± 0.03	0.18 ± 0.01
115.8	0.86 ± 0.04	0.21 ± 0.01
120.0	1.16 ± 0.06	0.31 ± 0.02
123.7	1.31 ± 0.07	0.31 ± 0.02
127.5	1.47 ± 0.07	0.38 ± 0.02
131.5	1.71 ± 0.09	0.48 ± 0.02
135.1	1.76 ± 0.09	0.51 ± 0.03
139.2	1.85 ± 0.09	0.59 ± 0.03
142.9	1.74 ± 0.09	0.54 ± 0.03
146.5	1.83 ± 0.09	0.60 ± 0.03
150.6	1.73 ± 0.09	0.62 ± 0.03
154.1	1.63 ± 0.08	0.55 ± 0.03
157.0	1.61 ± 0.08	0.55 ± 0.03

TABLE II. (*Continued*.)

Θ [deg]	$d\sigma/d\Omega^{\Delta Z=1}$ [mb/sr]	$d\sigma/d\Omega^{\Delta Z=2}$ [mb/sr]
$E_{lab}=57$ MeV		
131.4	0.22 ± 0.01	0.01 ± 0.01
135.0	0.25 ± 0.01	0.01 ± 0.01
139.1	0.30 ± 0.01	0.03 ± 0.01
142.7	0.31 ± 0.02	0.04 ± 0.01
146.4	0.39 ± 0.02	0.04 ± 0.01
150.5	0.44 ± 0.02	0.05 ± 0.01
154.0	0.45 ± 0.02	0.06 ± 0.01
156.9	0.49 ± 0.02	0.05 ± 0.01
$E_{lab}=56$ MeV		
134.3	0.09 ± 0.01	
138.1	0.10 ± 0.01	
141.9	0.16 ± 0.01	
145.5	0.14 ± 0.01	
149.3	0.23 ± 0.01	
153.0	0.18 ± 0.01	

rier. This figure also shows the data obtained by Yokoyama *et al.* [8] and by Eyal *et al.* [9] which were taken at much higher bombarding energies. Whereas the data of Eyal *et al.* [9] are consistent with the trend of the excitation functions measured in the present work, the results of Yokoyama *et al.* [8] in the $^{16}O+^{197}Au$ system at $E/V_c=1.83$ fall well above the values we have measured.

In what follows a semiclassical description of the transfer data will be given. In all cases, theoretical calculations have been done assuming one-proton- and two-proton-transfer reactions for $\Delta Z=1$ and $\Delta Z=2$, respectively. Morover, since the collected data also contain information from the quasielastic scattering, these results will be discussed in the framework of the optical model.

A. Semiclassical description of the transfer reactions

In a semiclassical approach, the differential transfer cross section at energies below the barrier is given by [10]

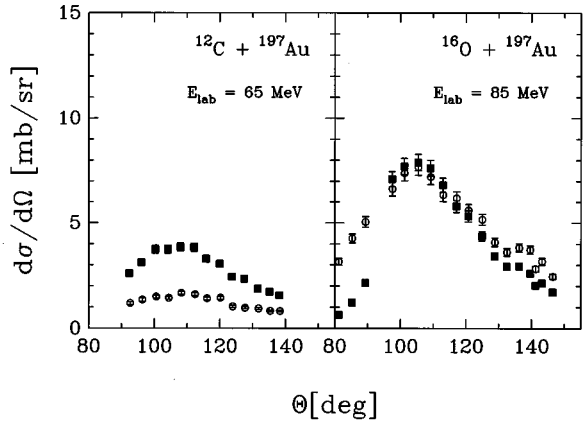

FIG. 4. Differential cross sections for transfer reactions measured in the $^{12}C+^{197}Au$ system at $E_{lab}=65$ MeV and $^{16}O+^{197}Au$ system at $E_{lab}=85$ MeV. Solid squares are one-charge-transfer and open circles are two-charge-transfer channels.

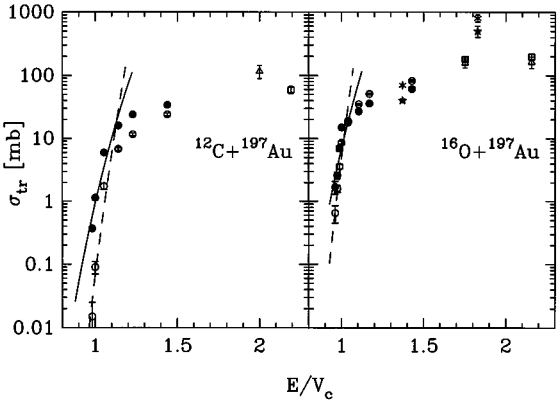

FIG. 5. Charged-particle-transfer cross sections for the $^{12}C+^{197}Au$ and $^{16}O+^{197}Au$ systems. Solid circles are one-charge-transfer and open circles are two-charge-transfer channels measured in this work, and open squares and triangles are one- and two-charge-transfer channels, respectively, from Ref. [9], while solid and open stars are one- and two-charge-transfer channels, respectively, from Ref. [8]. Solid and dashed lines are theoretical expectations from Eq. (7) for one- and two-proton stripping, respectively.

$$\left(\frac{d\sigma}{d\Omega}\right)_{tr}=P_{tr}(\Theta)\left(\frac{d\sigma}{d\Omega}\right)_{R}, \tag{1}$$

where $(d\sigma/d\Omega)_R$ denotes the differential reaction cross section and

$$P_{tr}(\Theta)=C\sin\left(\frac{\Theta}{2}\right)\exp\{-2\kappa D(\Theta)\} \tag{2}$$

is the transfer probability expected for nucleon tunneling between two potential wells as a function of the scattering angle Θ. The amplitude C depends, essentially, on the initial

TABLE III. Total transfer cross sections for one- and two-charge-stripping reaction channels for both systems.

System	E_{lab} [MeV]	$\sigma_{tr}^{\Delta Z=1}$ [mb]	$\sigma_{tr}^{\Delta Z=2}$ [mb]
$^{12}C+^{197}Au$			
	82	34 ± 2	24 ± 1
	70	24 ± 1	11.6 ± 0.6
	65	16.0 ± 0.8	6.8 ± 0.4
	60	6.0 ± 0.4	1.7 ± 0.2
	57	1.2 ± 0.1	0.09 ± 0.02
	56	0.4 ± 0.1	0.01 ± 0.01
$^{16}O+^{197}Au$			
	110	61 ± 4	82 ± 3
	90	36 ± 2	51 ± 1
	85	27 ± 1	35 ± 1
	80	18 ± 1	19.0 ± 0.7
	77	15.0 ± 0.7	8.6 ± 0.5
	76	7.0 ± 0.7	3.6 ± 0.3
	75	2.6 ± 0.3	1.6 ± 0.2
	74	1.7 ± 0.4	0.6 ± 0.2

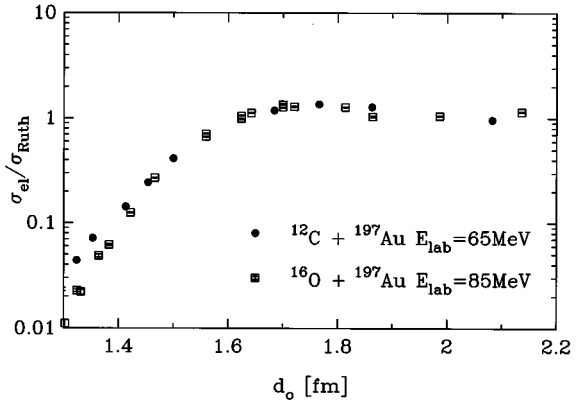

FIG. 6. Quasielastic cross section normalized to Rutherford cross section plotted as a function of the reduced radius parameter d_0 for the $^{12}C+^{197}Au$ (solid circles) and $^{16}O+^{197}Au$ (open squares) systems at $E_{lab}=$ 65 MeV and 85 MeV, respectively.

and final states as well as on the kinematics of the reaction. The value of the propagation number κ is defined through the WKB approximation as

$$\kappa=\frac{1}{\hbar(x_1-x_2)}\int_{x_1}^{x_2}\sqrt{2\mu[\mathcal{B}+U(r)]}dr, \tag{3}$$

where $\mathcal{B}$ is the binding energy of the transferred particle, μ is its reduced mass, and the integration limits x_i correspond to $\mathcal{B}+U(x_i)=0$. The total nucleon-nucleus potential $U(r)$ is defined as

$$U(r)=U_1(r)+U_2(D-r), \tag{4}$$

$$U_i(r)=U_{C_i}(r)+U_{N_i}(r). \tag{5}$$

Here the subscripts 1 and 2 refer to the donor and acceptor cores, respectively, D is the distance of closest approach between them, r is the position of the transferred particle with respect to the donor core, and U_{C_i} and U_{N_i} are the Coulomb potential and the nuclear potential, respectively. In the calculations we considered the Coulomb potential as that generated by a charged sphere of radius $R_{c_i}=1.25A_i^{1/3}$ fm and the nuclear part as a Woods-Saxon potential with parameters taken from Ref. [12]. Assuming Coulomb trajectories, $D(\Theta)$ is given by

$$D(\Theta)=\frac{e^2Z_pZ_t}{2E_{\text{c.m.}}}\left(1+\csc\frac{\Theta}{2}\right), \tag{6}$$

where Z_p and Z_t are the atomic number of the projectile and target, respectively.

For energies below the Coulomb barrier, the total transfer cross section σ_{tr} can be deduced from the distance of closest approach in a head-on collision, $D(\pi)$ [10],

$$\sigma_{tr}\sim\exp[-2\kappa D(\pi)]. \tag{7}$$

This theoretical expectation reproduces reasonably well the experimental data obtained in this work as can be seen in Fig. 5, where one- and two-proton-stripping reactions have been assumed in the calculations. Under the assumption of Eq. (6), the behavior of the transfer probability as a function of the distance of closest approach given by Eq. (2) has been verified for a variety of systems, although the observed values of the decay constants do not always agree with some expectations derived from the model described above [1,5].

Figure 6 exhibits the elastic data normalized to the Rutherford cross section, as a function of the reduced radius parameter $d_0=D/(A_1^{1/3}+A_2^{1/3})$. For $d_0>1.65$ fm, the ratio $\sigma_{el}/\sigma_{Ruth}$ remains equal to one. For $d_0<1.65$ fm this ratio falls off exponentially due to absorptive processes caused by

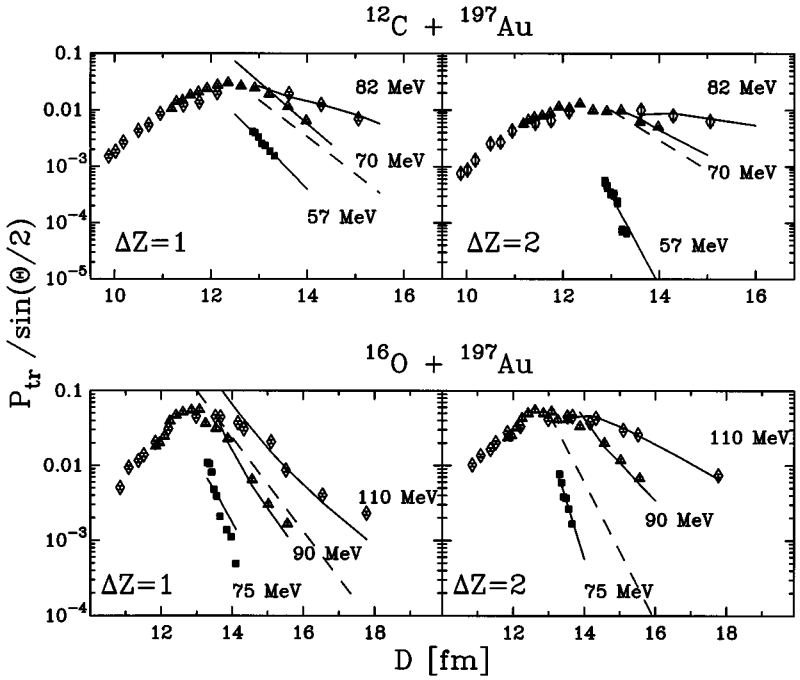

FIG. 7. Probabilities as a function of D for one- and two-charge-transfer channels in the $^{12}C+^{197}Au$ and $^{16}O+^{197}Au$ systems. Diamonds correspond to E_{lab} = 82 (110) MeV, triangles to E_{lab} = 70 (90) MeV, and squares E_{lab} = 57 (75) MeV for the $^{12}C+^{197}Au$ ($^{16}O+^{197}Au$) systems. Dashed lines are the theoretical expectations derived from Eq. (2), and solid lines are calculations explained in the text.

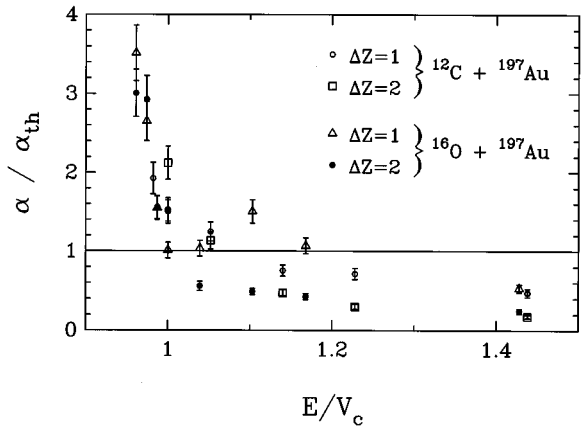

FIG. 8. One- and two-charge-transfer normalized slopes (see text) as a function of the bombarding energies normalized to the Coulomb barrier for the $^{12}C+^{197}Au$ and $^{16}O+^{197}Au$ systems.

the nuclear potential. This result agrees with that given in Ref. [5] and indicates the range of validity of the Coulomb trajectories in order to determine distances between projectile and target as a function of the scattering angle.

Figure 7 shows the experimental values of $P_{tr}/\sin(\Theta/2)$ as a function of the distance of closest approach $D(\Theta)$ derived from Coulomb trajectories for the different measured systems. The experimental probabilities P_{tr} for a given angle Θ are obtained from the measured differential transfer cross section and the corresponding Rutherford cross section using Eq. (1).

At sufficiently large internuclear distances the experimental points qualitatively follow the exponential decay predicted by Eq. (3). The theoretical slopes $\alpha_{th}=2\kappa$ for one- and two-proton-transfer probabilities are 1.51 (1.44) and 2.37 (2.12) fm^{-1}, respectively, for the $^{12}C+^{197}Au$ ($^{16}O+^{197}Au$) system, and they are represented by dashed lines in Fig. 7. However, whereas these theoretical slopes do not depend on the bombarding energy, the experimental slopes decrease with increasing energies.

This dependence can also be seen in Fig. 8, where the experimental slopes normalized to the energy-independent values, α/α_{th}, are displayed as a function of the reduced energy parameter E/V_c. The energy dependence is particularly strong near the barrier and becomes much flatter at the highest energies.

A possible explanation of this behavior might stem from the presence of the nuclear potential modifying the Coulomb trajectory [13,14]. In this case, several trajectories with different distances of closest approach may contribute to each angle Θ. We assume that the nuclei move along classical

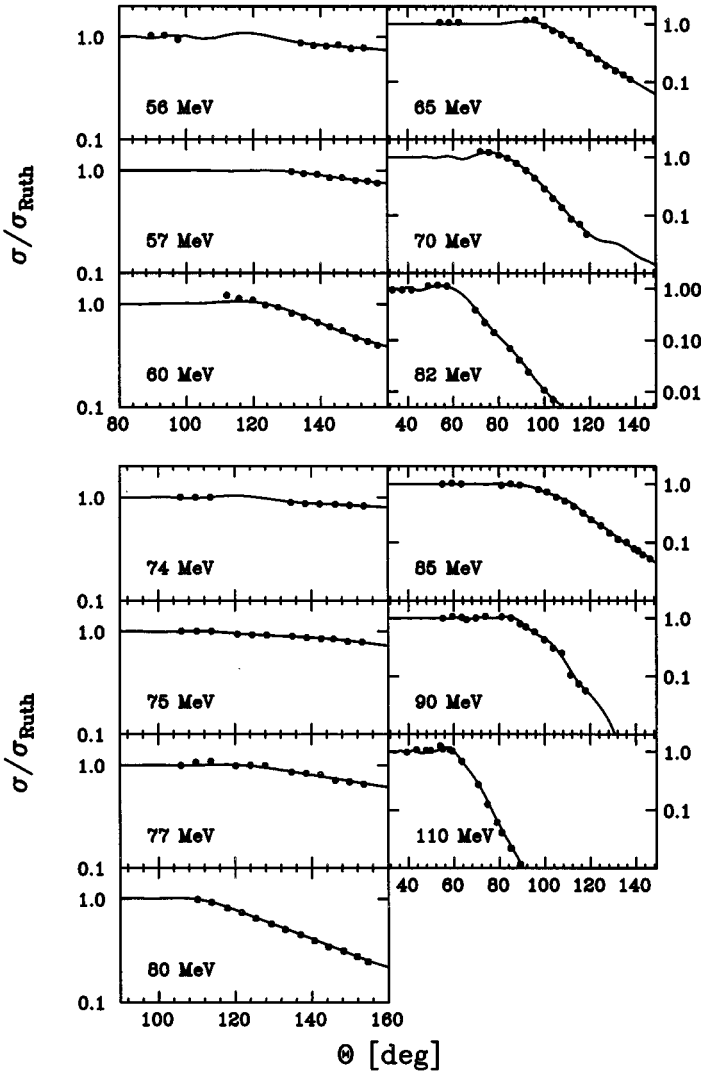

FIG. 9. Angular distributions for quasielastic scattering normalized to Rutherford cross section, for all energies measured in the $^{12}C+^{197}Au$ (upper panel) and $^{16}O+^{197}Au$ (lower panel) systems. Solid lines are the results of the optical model calculations described in the text.

TABLE IV. Optical model parameters fitted by the code PTOLEMY. The parameters R_{Sv} and R_{Sw} are the real and imaginary sensitivity radii, and V_S and W_S are the real and imaginary potentials evaluated at the sensitivity radius.

	E_{lab} [MeV]	V [MeV]	r_R [fm]	a_R [fm]	W [MeV]	r_I [fm]	a_I [fm]	R_{Sv} [fm]	R_{Sw} [fm]	V_S [MeV]	W_S [MeV]
^{12}C											
	56	21.6	1.36	0.57	0.57	1.40	0.60	11.3	11.5	4.43	0.20
	57	26.8	1.33	0.44	0.98	1.40	0.58	11.9	11.3	2.57	0.55
	60	23.1	1.33	0.42	2.05	1.40	0.13	11.9	11.5	2.18	1.54
	65	21.8	1.33	0.41	3.45	1.40	0.22	11.4	11.4	1.85	2.28
	70	17.4	1.33	0.45	3.73	1.40	0.13	12.1	11.4	1.83	2.59
	82	18.3	1.36	0.32	4.44	1.40	0.33	11.6	11.4	1.64	2.71
^{16}O											
	74	30.3	1.46	0.20	1.06	1.55	0.15	12.4	13.3	11.4	0.43
	75	31.9	1.45	0.14	0.97	1.55	0.33	12.8	13.6	8.3	0.43
	77	30.9	1.42	0.23	2.13	1.51	0.14	12.6	12.4	3.8	0.18
	80	34.0	1.43	0.21	2.96	1.50	0.14	12.8	12.9	1.2	0.21
	85	39.3	1.37	0.23	2.20	1.51	0.35	11.7	13.4	1.0	0.68
	90	32.6	1.34	0.29	1.91	1.52	0.20	12.6	12.8	0.9	0.40
	110	33.8	1.33	0.33	2.74	1.45	0.32	12.0	12.6	1.0	0.19

trajectories under the influence of the Coulomb potential and of the real part of the nuclear optical potential. For the latter we use a Woods-Saxon shape with radius and strength calculated as in Ref. [12]. Considering the absorption due to the imaginary part of the nuclear potential [15], the probability for tunneling through the potential barrier was determined as in Ref. [16]. The depth of the imaginary part of the optical potential was taken as the only free parameter in the calculation. This parameter, which was obtained from the simultaneous fit to the data from both systems at all energies, was determined to be $W_0 = 33.9$ MeV. It can be seen that for the optimum value of the strength parameter in the imaginary part of the optical potential the global trend of the energy dependence is well described. In Sec. III B we will further discuss the dependence of the results of these calculations upon the optical model parameters, in particular, in connection with those obtained from our quasielastic data. A more extensive description of this theoretical treatment can be found in Ref. [14].

The energy dependence of the slope α has been observed in the two-neutron-transfer reaction in the spherical ^{208}Pb $+ ^{28}$Si system but no energy dependence of the slope was observed for the one-neutron-transfer channel in the same system [17]. Similar results were reported by Rehm [17] for the ^{208}Pb$+ ^{58}$Ni, ^{36}S$+ ^{58}$Ni, and ^{58}Ni$+ ^{144,154}$Sm systems, and more recently Saha *et al.* [18] observed that the anomaly is present in one-proton-transfer reactions in the ^{28}Si$+ ^{68}$Zn system.

B. Optical model analysis

The interpretation of the transfer data in terms of the model outlined in the previous section can be also examined from the point of view of its consistency with the optical parameters derived from the quasielastic angular distributions. Besides, the wide range of bombarding energies covered in this study allowed us to investigate the energy dependence of the optical model potentials. This is closely related to the problem of the dispersion relation that links the real and imaginary parts of the nuclear potential.

Figure 9 shows the quasielastic angular distributions for ^{12}C$+ ^{197}$Au and ^{16}O$+ ^{197}$Au normalized to the Rutherford cross section. Because of the energy resolution of the telescope, these cross sections include elastic scattering and contributions from inelastic scattering and neutron transfer. These angular distributions were fitted using the code PTOLEMY [19] and the obtained optical model parameters are listed in Table IV. The calculated angular distributions are shown as solid lines in Fig. 9.

The dependence of the real and imaginary parts of the optical potential was also studied as a function of the bombarding energy. For that purpose, the potentials were evaluated at the so-called sensitivity radius, i.e., the distance at which the various potentials that fit the data take almost the same value and, therefore, this value can be determined with minimum ambiguity. The average real and imaginary sensitivity radii have been found to be $R_{Sv} = 11.7$ fm, $R_{Sw} = 11.4$ fm and $R_{Sv} = 12.3$ fm, $R_{Sw} = 13.0$ fm for ^{12}C$+ ^{197}$Au and ^{16}O$+ ^{197}$Au systems, respectively (the values may be considered as essentially constant even though it seems to be a small decreasing tendency with increasing bombarding energy).

The values of the real and imaginary potentials at the sensitivity radius (V_S and W_S) can be compared to the ones which best reproduce the transfer data using the parameters prescribed in Ref. [12]. Those potentials, evaluated at the sensitivity radius, are $V_S = 3.20$ MeV, $W_S = 2.71$ MeV for ^{12}C$+ ^{197}$Au and $V_S = 2.41$ MeV, $W_S = 0.47$ MeV for ^{16}O $+ ^{197}$Au. Although the results from both fits qualitatively

agree, it is worth mentioning that the optical model calculations using the potential parameters obtained from the transfer data do not succeed in reproducing the quasielastic angular distributions. In this comparison it should be noticed that the optical model potentials listed in Table IV are strongly energy dependent, whereas a single value was used at all energies for the transfer data.

Regarding the behavior of the potentials as a function of the bombarding energy, the parameters of Table IV in the case of $^{12}C+^{197}Au$ exhibit the general trend expected from a dispersion relation, namely, the observed increase in V_S and a decrease in W_S as the bombarding energy approaches the barrier from above (see Ref. [20] and references therein). In the case of $^{16}O+^{197}Au$ the real part of the optical potential shows also this behavior although the results for the imaginary part are much less certain.

IV. SUMMARY

Transfer reaction in the $^{16}O+^{197}Au$ and $^{12}C+^{197}Au$ systems were measured at energies close to the Coulomb barrier with charge identification. The angular distributions for elastic, one-charge-, and two-charge-transfer reactions were used to obtain the transfer probabilities and the total transfer cross sections. The measured transfer probabilities are not in agreement with the semiclassical model that assumes tunneling from Coulomb trajectories.

ACKNOWLEDGMENTS

Some of us (J.O.F.N., A.J.P., J.E.T., D.E.D.G, and M.d.T.) acknowledge the financial support of the Consejo Nacional de Investigaciones Científicas y Técnicas, Argentina.

[1] A.O. Macchiavelli, M.A. Deleplanque, R.M. Diamond, F.S. Stephens, E.L. Dines, and J.E. Draper, Nucl. Phys. **A432**, 436 (1985).

[2] S. Juutinen, X.T. Liu, S. Sorensen, B. Cox, R.W. Kincaid, C.R. Bingham, M.W. Guidry, W.J. Kernan, C.Y. Wu, E. Vogt, T. Czosnyka, D. Cline, M.L. Halbert, I.Y. Lee, and C. Baktash, Phys. Lett. B **192**, 307 (1987).

[3] A.H. Wuosmaa, K.E. Rehm, B.G. Glagola, Th. Happ, W. Kutschera, and F.L.H. Wolfs, Phys. Lett. B **255**, 316 (1991).

[4] R.B. Roberts, S.B. Gazes, J.E. Mason, M. Satteson, S.G. Teichmann, L.L. Lee, J.F. Liang, J.C. Mahon, and R.J. Vojtech, Phys. Rev. C **47**, 1831 (1993).

[5] K.E. Rehm, B.G. Glagola, W. Kutschera, F.L.H. Wolfs, and A.H. Wuosmaa, Phys. Rev. C **47**, 2731 (1993).

[6] C.Y. Wu, X.T. Liu, W.J. Kernan, D. Cline, T. Czosnyka, M.W. Guidry, A.E. Kavka, R.W. Kincaid, B. Kotlinski, S.P. Sorensen, and E. Vogt, Phys. Rev. C **39**, 298 (1989).

[7] W.J. Kernan, C.Y. Wu, X.T. Lui, H.L. Lan, D. Cline, T. Czosnyka, M.W. Guidry, M.L. Halbert, S. Juutinen, A.E. Kavka, R.W. Kincaid, J.O. Rasmussen, S.P. Sorensen, M.A. Stoyer, and E.G. Vogt, Nucl. Phys. **A524**, 344 (1991).

[8] A. Yokoyama, T. Saito, H. Baba, K. Hata, Y. Nagame, S. Ichikawa, S. Baba, A. Shinohara, and N. Imanishi, Z. Phys. A **332**, 71 (1989).

[9] Y. Eyal, K. Beg, D. Logan, J. Miller, and A. Zebelman, Phys. Rev. C **8**, 1109 (1973).

[10] R. Bass, *Nuclear Reactions with Heavy Ions* (Springer-Verlag, Berlin, 1980).

[11] M. Lederer and V.S. Shirley, *Table of Isotopes*, 7th ed. (John Wiley & Sons, New York, 1978).

[12] R.A. Broglia and A. Winther, *Heavy Ion Reactions* (Addison-Wesley, Reading, MA 1991).

[13] H.J. Kim, J. Gómez del Campo, M.M. Hindi, D. Shapira, and P.H. Stelson, Phys. Rev. C **38**, 2081 (1988).

[14] H. D. Marta, R. Donangelo, D. Tomasi, J.O. Fernández Niello, and A.J. Pacheco (unpublished).

[15] L.F. Canto, R. Donangelo, R.S. Nikam, and P. Ring, Phys. Lett. B **192**, 4 (1987).

[16] L.C. Vaz and J.M. Alexander, in *Proceedings of the International Conference Held at the MIT*, Cambridge, MA, 1984, edited by S.G. Steadman (Springer-Verlag, Berlin, 1985), p. 288.

[17] K.E. Rehm, in *Proceedings of the XII Workshop on Nuclear Physics*, Iguazu Falls, Argentina, 1989, edited by M.C. Cambiaggio, A.J. Kreiner, and E. Ventura (World Scientific, Singapore, 1990).

[18] S. Saha, Y.K. Agarwal, and C.V.K. Baba, Phys. Rev. C **49**, 2578 (1994).

[19] M.J. Rhoades-Brown, M.H. MacFarlane, and S.C. Pieper, Phys. Rev. C **21**, 2417 (1980).

[20] D. Abriola, A.A. Sonzogni, M. di Tada, A. Etchegoyen, M.C. Etchegoyen, J.O. Fernández Niello, S. Gil, A.O. Macchiavelli, A.J. Pacheco, R. Piegaia, and J.E. Testoni, Phys. Rev. C **46**, 244 (1992).